Word count: 39,201

Revision 1

Pyradoketosite, a new, unexpected, polymorph of Ag_3SbS_3 from the Monte Arsiccio mine (Apuan Alps, Tuscany, Italy)

CRISTIAN BIAGIONI[1,*], LUCA BINDI[2], YVES MOËLO[3], CHRISTOPHER J. STANLEY[4], FEDERICA ZACCARINI[5]

[1] *Dipartimento di Scienze della Terra, Università di Pisa, Via S. Maria 53, I-56126 Pisa, Italy*
[2] *Dipartimento di Scienze della Terra, Università degli Studi di Firenze, Via G. La Pira 4, I-50121 Firenze, Italy*
[3] *Université de Nantes, CNRS, Institut des Matériaux Jean Rouxel, IMN, F-44000 Nantes, France*
[4] *Department of Earth Sciences, Natural History Museum, London, SW 7 5BD, United Kingdom*
[5] *Department of Applied Geological Sciences and Geophysics, University of Leoben, Peter Tunner Str. 5, A-8700 Leoben, Austria*

**e-mail address: cristian.biagioni@unipi.it*

This is the peer-reviewed, final accepted version for American Mineralogist, published by the Mineralogical Society of America.
The published version is subject to change. Cite as Authors (Year) Title. American Mineralogist, in press.
DOI: https://doi.org/10.2138/am-2022-8136. http://www.minsocam.org/

ABSTRACT

Although everything seemed clear about the Ag–Sb–S compounds belonging to one of the more deeply studied experimental systems, nature allowed us to discover a new polymorph of Ag_3SbS_3, which could represent a compound for assessing new technological potentialities. The new mineral species pyradoketosite, Ag_3SbS_3 (IMA 2019-132), was discovered in the pyrite + baryte + iron oxide ore deposit of the Monte Arsiccio mine, Apuan Alps, Tuscany, Italy. It occurs as brittle orange acicular crystals, up to 200 μm in length and 25 μm in thickness, with adamantine luster. Under reflected light, pyradoketosite is slightly bluish grey, with abundant orange internal reflections. Bireflectance is weak and anisotropism was not observed, being masked by abundant internal reflections. Minimum and maximum reflectance data for the wavelengths recommended by the Commission on Ore Mineralogy [R_{min}/R_{max} (%), (λ, nm)] are: 32.8/32.9 (470), 30.2/30.7 (546), 29.0/29.6 (589), and 27.5/28.4 (650). Electron microprobe analysis gave (mean of 6 spot analyses, in wt%): Ag 59.81, Sb 22.63, S 17.78, total 100.22. On the basis of (Ag+Sb) = 4 atoms per formula unit, the empirical formula of pyradoketosite is $Ag_{2.996(11)}Sb_{1.004(11)}S_{2.996(15)}$. Pyradoketosite is monoclinic, space group $P2_1/n$, with a = 13.7510(15), b = 6.9350(6), c = 19.555(2) Å, β = 94.807(4)°, V = 1858.3(3) Å^3, Z = 12. The crystal structure was solved and refined to R_1 = 0.063 on the basis of 2682 unique reflections with $F_o > 4\sigma(F_o)$ and 191 refined parameters. The crystal structure of pyradoketosite can be described as formed by the alternation of {101} layers: an Sb-rich layer, Sb_3AgS_3, and two distinct Ag_8S_6 layers. This layered organization allows to identify structural relationships with the wittichenite-skinnerite pair. Pyradoketosite is associated with pyrargyrite, tetrahedrite-(Hg), valentinite, and probable pyrostilpnite in baryte + dolomite + quartz veins embedded in metadolostone. Its name derives from the old Greek words "πυρ" (fire) and "άδόκητος" (unforeseen), owing to the unexpected occurrence of this third polymorph of the compound Ag_3SbS_3.

45 *Key-words*: pyradoketosite, silver, antimony, sulfosalt, crystal structure, new mineral, Monte
46 Arsiccio mine, Apuan Alps, Tuscany, Italy.

47

INTRODUCTION

More than 150 Ag-chalcogenides are currently known as valid mineral species, mainly represented by sulfosalts (e.g., Moëlo et al. 2008; Bindi and Biagioni 2018). Indeed, silver is a chemical constituent of several minerals belonging to important groups of sulfosalts, e.g., sartorite (Makovicky and Topa 2015), lillianite (e.g., Makovicky and Topa 2014), polybasite (e.g., Bindi et al. 2007, 2020), and tetrahedrite (Biagioni et al. 2020b) groups. Despite the wide number of mineral species, the Ag–Sb–S system currently has only six approved sulfosalts, i.e., baumstarkite, cuboargyrite, miargyrite, pyrargyrite, pyrostilpnite, and stephanite. Baumstarkite (triclinic), cuboargyrite (cubic), and miargyrite (monoclinic) can be considered as polymorphs of the compound $AgSbS_2$ (Smith et al. 1997; Walenta 1998; Effenberger et al. 2002), although Kitakaze et al. (2006) questioned the dimorphic relations between baumstarkite and miargyrite. Trigonal pyrargyrite and monoclinic pyrostilpnite are the two known dimorphs of Ag_3SbS_3 (Laufek et al. 2010; Biagioni et al. 2020c), with the latter being the low-*T* polymorph (e.g., Chang 1963; Keighin and Honea 1969). Stephanite, Ag_5SbS_4, is another low-*T* Ag-sulfosalt, stable below 197 ± 5°C (e.g., Keighin and Honea 1969), with orthorhombic symmetry (Leitl et al. 2009).

During the study of the sulfosalt assemblages of the Monte Arsiccio mine (Apuan Alps, northern Tuscany, Italy), two samples showing μm-sized acicular crystals, orange in color, were observed. Electron microprobe and single-crystal X-ray diffraction studies showed it to be a new polymorph of Ag_3SbS_3. The mineral and its name were approved by the Commission on New Minerals, Nomenclature and Classification of the International Mineralogical Association (CNMNC-IMA) under the number IMA 2019-132. Holotype material is deposited in the mineralogical collection of the Museo di Storia Naturale, Università di Pisa, Via Roma 79, Calci, Pisa (Italy), under catalogue number 19913. The name pyradoketosite alludes to the unforeseeable nature of this mineral and it is formed from the old Greek words "πυρ" (fire) and "άδόκητος"

(unforeseen); the name also reflects the surprise at finding a new polymorph of the "ruby silvers" Ag_3SbS_3, as both the dimorphs pyrargyrite and pyrostilpnite have been known for a long time.

This paper describes this new silver sulfosalt and discusses its relationships with the other known "ruby silvers" as well as with the members of the wittichenite-skinnerite group having structural similarities with pyradoketosite.

OCCURRENCE AND MINERAL DESCRIPTION

Pyradoketosite is very rare and was identified in only two specimens from the Sant'Olga level, Monte Arsiccio mine (latitude 43°58'N, longitude 10°17'E), Apuan Alps, northern Tuscany, Italy. This mine exploited, up to the end of the 1980s, a pyrite + baryte + iron oxide (magnetite, hematite, "limonite") ore deposit located close to the contact between a Paleozoic metasedimentary-metavolcanic sequence and Triassic metadolostone, in the north-eastern sector of the Sant'Anna tectonic window. The Monte Arsiccio mine is the type locality for nine other mineral species, among which are some other sulfosalts: boscardinite (Orlandi et al. 2012), protochabournéite (Orlandi et al. 2013), arsiccioite (Biagioni et al. 2014), and andreadiniite (Biagioni et al. 2018). Pyradoketosite is the tenth new mineral discovered at this locality. A review of the geological setting of this mine is given in Biagioni et al. (2020a) and references therein.

Pyradoketosite occurs as acicular crystals, striated parallel to the elongation, up to 200 μm in length and 25 μm in thickness (Figure 1). Color and streak are orange. The mineral is translucent, with an adamantine luster. Owing to the small size and extreme rarity of pyradoketosite, hardness was not measured. This mineral is brittle. No cleavage was observed. Density was not measured; on the basis of the empirical formula and unit-cell parameters refined from single-crystal X-ray diffraction data, the calculated density is 5.809 g/cm^3.

Under reflected light, pyradoketosite is slightly bluish grey in color, with abundant orange internal reflections. Pleochroism was not observed. Bireflectance is weak and anisotropism was not

observed, being masked by abundant internal reflections. Pyradoketosite is weakly light sensitive. Reflectance values (SiC as standard) were measured in air (Natural History Museum, London) and are reported in Table 1 and shown in Figure 2.

Pyradoketosite occurs in baryte + dolomite + quartz veins, in association with valentinite, a tetrahedrite-group mineral [likely tetrahedrite-(Hg), on the basis of energy dispersive spectrometry (EDS) data collected on an unpolished grain], and some unidentified phases. In one sample, pyradoketosite occurs in a dissolution cavity of a previous unknown sulfosalt, along with valentinite. Figure 1 shows the close association of the acicular crystal of pyradoketosite with two other phases. Both have the same chemical composition as pyradoketosite. One of them, forming equant crystals, with a trigonal symmetry, was identified as pyrargyrite, on the basis of single-crystal X-ray diffraction data, whereas the other, characterized by a tabular habit, is tentatively attributed to pyrostilpnite on the basis of crystal morphology.

CHEMICAL DATA

Preliminary chemical analyses of pyradoketosite performed through EDS showed Ag, Sb and S as the only elements with $Z > 8$. Quantitative data were obtained through wavelength dispersive spectrometry (WDS mode) with a Superprobe JEOL JXA8200 electron microprobe at the "Eugen F. Stumpfl laboratory", Leoben University, Austria, using the following analytical conditions: accelerating voltage 20 kV, beam current 10 nA, nominal beam diameter 1 μm. The peak and backgrounds counting times were 15 and 5 seconds, respectively. The following standards (element, emission line) were used: electrum $Ag_{70}Au_{30}$ (Ag*L*α) and stibnite (S*K*α, Sb*L*α). Chemical data are given in Table 2. The empirical formula, based on 4 (Ag + Sb) atoms per formula unit (apfu), is $Ag_{2.996(11)}Sb_{1.004(11)}S_{2.996(15)}$. The ideal formula of pyradoketosite, Ag_3SbS_3, corresponds to (in wt%): Ag 59.76, Sb 22.48, S 17.76, total 100.00.

X-RAY CRYSTALLOGRAPHY AND STRUCTURE REFINEMENT

The X-ray powder diffraction pattern of pyradoketosite was collected using a 114.6 mm diameter Gandolfi camera and Ni-filtered Cu*K*α radiation. Owing to the very small size of the available material, the observed pattern showed only few and weak diffraction lines despite the long exposure time (one week). Table 3 reports the observed X-ray powder diffraction pattern along with that calculated on the basis of the structural model described below.

Single-crystal X-ray diffraction data were collected using a Bruker Smart Breeze three-circle diffractometer equipped with an air-cooled Photon II CCD detector, with graphite-monochromatized Mo*K*α radiation (Dipartimento di Scienze della Terra, Università di Pisa). The detector-to-crystal distance was set at 50 mm. A total of 1072 frames were collected in ω scan mode in 0.5° slices, with an exposure time of 25 s per frame. Intensity data were corrected for Lorentz-polarization factors, absorption and background using the package of software *Apex*3 (Bruker AXS Inc. 2016).

Pyradoketosite is monoclinic, with unit-cell parameters a = 13.7510(15), b = 6.9350(6), c = 19.555(2) Å, β = 94.807(4)°, V = 1858.3(3) Å^3. The a:b:c ratio is 1.9828:1:2.8198. The analysis of the reflection conditions led unequivocally to the choice of the space group $P2_1/n$. This cell can be transformed in the standard space group $P2_1/c$ through the matrix $\boldsymbol{R}$ = [1 0 0 | 0 -1 0 | -1 0 -1], resulting in the unit-cell parameters a = 13.7510(15), b = 6.9350(6), c = 22.944(2) Å, β = 121.864(5)°, V = 1858.3(3) Å^3. However, the more orthogonal $P2_1/n$ space group was preferred, and the crystal structure was solved in this space group through direct methods using *Shelxs*-97 and refined using *Shelxl*-2018 (Sheldrick 2015). Neutral scattering curves for Ag, Sb, and S were taken from the International Tables for Crystallography (Wilson 1992). The crystal structure solution allowed the location of twelve independent Ag and Sb sites, whereas following difference-Fourier syntheses led to the finding of nine S positions. The isotropic refinement converged to R_1 = 0.14, thus suggesting the correctness of the structural model. Owing to the similar scattering factors of Ag

147 (Z = 47) and Sb (Z = 51), these two atoms were located on the basis of their coordination
148 environment and bond-valence sums (BVS). All sites were found to be fully occupied. After several
149 cycles of anisotropic refinement for all atoms, the final statistical factor R_1 converged to 0.0626 for
150 2682 unique reflections with $F_o > 4\sigma(F_o)$ and 191 refined parameters.

151 Given the relatively large atomic displacement parameters (ADP) of some of the Ag atoms (as
152 typical of fast ion conducting phases - the average ADP values of the nine Ag positions was 0.046
153 Å^2, to be compared with 0.019 Å^2 for the three Sb sites), an attempt to refine the crystal structure
154 using higher order tensor elements in the expression of the structure factor (the "non harmonic
155 approach" – Johnson and Levy 1974; Zucker and Schulz 1982) was tried. As documented by Bindi
156 and Evain (2007), this alternative approach, in particular the Gram-Charlier formalism which is
157 recommended by the IUCr Commission on Crystallographic Nomenclature (Trueblood et al. 1996),
158 provides an easier convergence on the refinement, due to much lower correlations between the
159 refined parameters. The new refinement was carried out using the software JANA2006 (Petříček et
160 al. 2006). However, the occurrence of negative regions in the probability density function maps
161 indicated the inadequacy of the results. Consequently, the Gaussian approximation was preferred.

162 Details of the intensity data collection and crystal structure refinement are given in Table 4.
163 Selected bond distances are listed in Table 5. Bond-valence sums, calculated using the bond
164 parameters of Brese and O'Keeffe (1991), are shown in Table 6. The Crystallographic Information
165 File (CIF), including atomic coordinates and reflection data, is available as Supplementary Material.
166

167 ## CRYSTAL STRUCTURE ANALYSIS

168 ### Crystal structure description

169 The crystal structure of pyradoketosite (Fig. 3) shows the presence of twelve cation sites and
170 nine anion positions. Among the cation sites, nine are occupied by Ag^+ and three by Sb^{3+}. Two
171 different but complementary approaches can be used for the description of the crystal structure, i.e.,

according to the distribution of strong (= short) and weak (= long) bonds, or cutting the structure according to {101} layers having different chemical compositions.

Considering the shortest (= strongest) bonds, isolated SbS_3 trigonal pyramids can be observed organized according to {101} layers, with the pyramidal vertices alternately oriented towards [10-1] and [101] (Fig. 3). Antimony atoms show average <Sb–S> distances ranging between 2.429 Å and 2.465 Å (Table 5), comparable with 2.444 Å and 2.460 Å for pyrargyrite and pyrostilpnite (Laufek et al. 2010; Biagioni et al. 2020c), respectively. The BVS of Sb atoms (Table 6) ranges between 2.88 and 3.19 valence units (v.u.).

In Figure 3, {-102} layers sub-perpendicular to SbS_3 layers can be observed. One slab is partly represented in Figure 4. The Ag atom hosted at the Ag(2) site forms two strong bonds with two symmetry-related S(4) atoms (at 2.46 and 2.47 Å) and a longer bond at 2.72 Å with S(7). These S atoms belong to three different $Sb(2)S_3$ groups. In this way, an $[Ag(2)Sb(2)S_3]^{2-}$ ribbon can be distinguished. In this ribbon, Ag(2) atoms form with S(4) atoms a zig-zag chain running along **b**, decorated on both sides by $Sb(2)S_3$ trigonal pyramids. An additional longer bond at 2.86 Å completes the coordination environment of Ag(2). A similar configuration involves Ag(9) atoms, forming with S(2) atoms a zig-zag chain decorated by $Sb(1)S_3$ trigonal pyramids. It gives the ribbon $[Ag(9)Sb(1)S_3]^{2-}$.

The $Sb(3)S_3$ group shares its three S atoms with Ag atoms hosted at Ag(3). Along **b**, $Sb(3)S_3$ groups and Ag(3) alternate, forming a rod of composition $[Ag(3)Sb(3)S_3]^{2-}$. This rod is connected to the adjacent $[Ag(2)Sb(2)S_3]^{2-}$ ribbon through the Ag(1) site, whereas it is bonded to the $[Ag(9)Sb(1)S_3]^{2-}$ ribbon through the Ag(4) site (Fig. 4). Both Ag(1) and Ag(4) sites have a three-fold coordination. However, the coordination of Ag(1) is increased to four owing to the occurrence of an additional longer bond at 2.96 Å. The bonding of the (Ag/Sb) rod and the two (Ag/Sb) ribbons gives rise to the {-102} layer with chemical composition $[Ag_5Sb_3S_9]^{4-}$ (Fig. 3). Such layers are bonded along [-101] owing to the occurrence of three-fold coordinated Ag atoms hosted at the

Ag(5), Ag(6), Ag(7), and Ag(8) sites (Fig. 3). Considering all Ag atoms, average <Ag–S> distances range between 2.525 Å for the three-fold coordinated Ag(9) site and 2.629 Å for the four-fold coordinated Ag(2) position (Table 5). The BVS at the Ag sites varies between 0.94 and 1.22 v.u. (Table 6). The shortest Ag–Ag distance is 2.970(2) Å for the pair Ag(3)–Ag(7). The Ag–Sb distances are usually longer than 3.30 Å; however, a very short Ag–Sb distance occurs for the pair Ag(3)–Sb(1), i.e., 2.966(2) Å. This short distance may be indicative of an average position of the Ag(3) atom which could not be resolved in two sub-positions.

An alternative description of the crystal structure of pyradoketosite considers the occurrence of chemically different {101} layers. Figure 5 shows the organization of the crystal structure according to this {101} layered arrangement. This description is particularly useful in pointing out the relationship between pyradoketosite and the members of the wittichenite-skinnerite group (see below).

The crystal-chemical formula of pyradoketosite, derived from the crystal structure study, is Ag_3SbS_3 ($Z = 12$).

Comparison with other $Ag_3Sb\mathit{Ch}_3$ (*Ch* = S, Se) compounds

The compound Ag_3SbS_3 is known in nature since the 19th Century as pyrargyrite (trigonal, $R3c$) and pyrostilpnite (monoclinic, $P2_1/c$). The replacement of Sb by As gives rise to proustite, showing isotypic relations with pyrargyrite, and xanthoconite (monoclinic, $C2/c$) (e.g., Bindi and Biagioni 2018 and references therein). Eckerite, ideally $CuAg_2AsS_3$, is a Cu-bearing isotype of xanthoconite (Bindi et al. 2015). Table 7 compares pyradoketosite with these natural phases and with the three synthetic Ag-compounds having a similar stoichiometry.

The crystal structure of pyradoketosite is different from those of the other two naturally-occurring polymorphs, pyrargyrite (and its Se synthetic isotype) and pyrostilpnite, as well as from those of the synthetic orthorhombic Ag_3XSe_3 phases, where X = As, Sb. The crystal structure of

pyrargyrite is characterized by columns of SbS_3 pyramids running along **c**, with the orientation of their vertices preserved along the polar three-fold **c** axis. Silver atoms have a linear two-fold coordination and give rise to spirals running along [001] (Engel and Nowacki 1966; Laufek et al. 2010). In pyrostilpnite, {010} (Ag/Sb) layers, corresponding to $(210)_{PbS}$ slabs, run along **c** and are connected through longer Ag–S bonds (Kutoglu 1968; Biagioni et al. 2020c). Antimony atoms decorate these layers, and the lone-electron-pairs are directed in the space between successive layers along **b**. The coordination number of Ag atoms in pyrostilpnite varies from two to four. As described above, the crystal structure of pyradoketosite can be described as formed by {-102} layers connected by additional Ag atoms. Silver coordination is mainly triangular, with only one atom at the Ag(2) site having two-fold coordination.

A different packing density is also suggested by the calculation of the cell volumes for one Ag_3SbS_3 unit. Pyradoketosite is slightly less-densely packed (V = 154.8 Å^3) with respect to pyrargyrite (V = 153.6 Å^3) and pyrostilpnite (V = 152.1 Å^3). This is reflected by the calculated densities, increasing from pyradoketosite (5.81 g/cm^3) to pyrostilpnite (5.97 g/cm^3), passing through pyrargyrite (5.86 g/cm^3).

Relationship with the wittichenite-skinnerite homeotypic pair

On the basis of the Sb layering described in Figure 5, a supercell has been selected. This supercell can be derived from the $P2_1/n$ cell through the transformation matrix $\boldsymbol{R}$ = [1 0 -1| 0 1 0| 1 0 1] which gives the unit-cell parameters a = 24.831(2), b = 6.9350(6), c = 22.944(2) Å, β = 109.835(8)°, V = 3716.6(6) Å^3. It shows the alternation with the Sb-rich layer, $AgSb_3S_3$, of two distinct Ag_8S_6 layers (A and B). Considering the distribution of short (= strong) Ag–S distances (Ag–S < 2.75 Å), each Ag_8S_6 layer can be considered as the sum of $2Ag_3S_2 + Ag_2S_2$. Such an organization directly relates to the crystal structure of the wittichenite-skinnerite homeotypic pair (Moëlo et al. 2008). The crystal structure of wittichenite was independently solved by Matzat

(1972) and Kocman and Nuffield (1973) (Fig. 6a), whereas that of skinnerite was solved by Pfitzner (1994) and Makovicky and Balić-Žunić (1995) (Fig. 6b). One BiS or SbS layer alternates with one Cu_3S_2 layer. BiS and SbS layers are equivalent, while Cu distribution differs between the two structures.

Two synthetic Li-sulfides, Li_3SbS_3 and Li_3AsS_3, relate to this group (Huber et al. 2012) and are isotypic (Fig. 6c). The coordination of Li atoms is tetrahedral (two positions) or square pyramidal (one position), whereas Cu coordination in wittichenite and skinnerite is exclusively triangular.

Table 8 compares the unit-cell parameters of all these compounds. For the reduced unit cell (basis: 4 formula units), the stacking parameter is close to 10 Å, and the two in-plane parameters are close to 8 and 6.8 Å. Unit-cell volumes are in the range 530-545 $Å^3$. For "average pyradoketosite" (i.e., the reduced cell containing 4 formula units), Ag-for-Cu substitution increases all parameters relative to skinnerite: b + 12%, a + 6%, c + 4.5%, V + 17%.

Pyradoketosite appears as a derivative of wittichenite with a (2 × 3) superstructure (Table 8), with developed crystal chemical formula $(Ag_3S_2)_2(Ag_2S_2)(Sb_3AgS_3) = Ag_9Sb_3S_9$. In the other members of this group, while the (Bi/Sb/As)S layers are topologically identical, the adjustment of the intercalated $(Cu/Li)_3S_2$ layer proceeds in two different ways. In wittichenite and skinnerite, Cu coordination is triangular (ideal Cu–S distance: 2.27 Å), whereas in Li_3SbS_3, there are two LiS_4 tetrahedra and one LiS_5 square pyramid (ideal Li–S distances: 2.45 and 2.55 Å, respectively). In pyradoketosite, with Ag coordination mainly triangular (ideal Ag–S distance: 2.56 Å), due to the increase of the size of Ag^+ relatively to Cu^+ or Li^+, the steric adjustment is realized through the transfer of one Ag atom among nine from the Ag_3S_2 layer to the SbS layer, reducing the expansion of the former layer and expanding the latter. Pyradoketosite is a plesiotypic derivative of wittichenite, according to the definition of Makovicky (1997).

The uneven intra-layer superstructure (× 3) imposes a monoclinic stacking. The differentiation of two distinct Ag_8S_6 layers (A and B) results from Ag(3) pairing across the A layer (double black arrow in Figure 5), giving an Ag–Ag distance of 5.39 Å and, inversely, a longer distance across the B layer (8.17 Å).

GENESIS OF PYRADOKETOSITE

The occurrence of pyradoketosite reveals that unexpected complex crystal structures can occur in the Ag–Sb–S system. Details of this chemical system have been studied since the 1930s (see Keighin and Honea 1969 and references therein). Several researchers tried to describe the relationships between the products of experimental runs and the observed mineral assemblages, to use some of them as geothermometers. Pyrargyrite, the most common polymorph of Ag_3SbS_3, has been easily obtained in several synthesis experiments (e.g., Barstad 1959; Keighin and Honea 1969; Hoda and Chang 1975). On the contrary, pyrostilpnite was reported by Weil and Hocart (1953) in a synthesis carried out under glycerol. Their results, however, could not be reproduced by Keighin and Honea (1969). Chang (1963) observed that pyrostilpnite can invert into pyrargyrite under heating at 197°C for 300 h; on the contrary, pyrargyrite, heated at 150°C for 350 h, does not invert to pyrostilpnite. Keighin and Honea (1969) proposed an inversion temperature of 192 ± 5°C for the pyrostilpnite-pyrargyrite transition. It is worth noting that these authors underlined the experimental difficulties in attaining equilibrium assemblages, related to the sluggishness of the reaction kinetics below 300°C, requiring long-term runs (longer than one year), with the possible formation of non-equilibrium assemblages.

In this respect, the occurrence of pyradoketosite is an interesting conundrum. Such a phase, to the best of our knowledge, has not been obtained in any synthetic run (e.g., Goodell 1975 and references therein). Moreover, the crystal-chemical study excludes the possible role of minor constituents in the crystallization of pyradoketosite. The close examination of the spatial relations

between the three Ag_3SbS_3 polymorphs shown in Figure 1 can help in putting forward some hypotheses. Pyradoketosite is apparently overgrown by probable pyrostilpnite, whereas the latter is overgrown by the equant crystal of pyrargyrite. A first hypothesis could be that this association may represent the result of the co-precipitation of the three Ag_3SbS_3 polymorphs. On the contrary, taking into account the spatial relations among the three phases and considering that pyrostilpnite should invert to pyrargyrite above 192 ± 5°C, one could suppose that the sequence pyradoketosite → pyrostilpnite → pyrargyrite could be the result of an ephemeral prograde variation of *T*, not able to invert the low-*T* polymorphs into pyrargyrite. However, the role of other physical-chemical parameters (e.g., *p*H, Eh) or kinetic factors is currently unknown. Biagioni et al. (2020a) reported the results of microthermometric investigations performed on fluid inclusions hosted in quartz crystals from the same kind of baryte + dolomite ± quartz veins (occurrence of type C following Biagioni et al. 2020a) where pyradoketosite was found. In these veins, two generations of fluid inclusions occur. The first one has a modal homogenization temperature of 275°C (range 265-289°C), whereas a second generation of fluid inclusion homogenizes at 235°C (range 222-246°C). Pyradoketosite was observed in dissolution cavities, along with valentinite, and seems to be a late-stage mineral. Consequently, its crystallization may be due to a late-stage hydrothermal event, possibly corresponding to the second generation of fluid inclusions hosted in quartz crystals or to a later-stage (and likely cooler) event not recorded in the samples studied by Biagioni et al. (2020a).

IMPLICATIONS

One of the main questions for Mineralogy of the 21st Century is about the role played by the description of new mineral species. More and more Earth scientists consider this endeavor as a trivial, not important job, mainly because of the usual uniqueness of the discovered new minerals and their volumetric insignificance, apparently not playing any fundamental role in the Earth dynamics. For instance, the finding of pyradoketosite is limited to just a few crystals, with a total

321 volume less than 1 mm^3, thus fitting the definition of rarity given by Hazen and Ausubel (2016),
322 and its crystallization is likely constrained by a narrow *P-T-X* space. However, samples of
323 pyrostilpnite exhibiting an acicular morphology could have been misidentified and actually be
324 pyradoketosite.

325 In our opinion, the description of a new, rare mineral species as, for instance, pyradoketosite
326 cannot be considered as a mere crystal chemical exercise. Its finding improves our knowledge of the
327 Ag–Sb–S system, where the ternary compounds $AgSbS_2$ and Ag_3SbS_3 are actively used for their
328 thermoelectric properties as well as for their potential optical applications. Yet, pyrargyrite has long
329 been considered as a promising functional material for several opto-electronic and data storage
330 applications (e.g., Adler 1980) and its physical and thermodynamic properties have been deeply
331 investigated (e.g., Lange et al. 1993; Schönau and Redfern 2002; Aspiala et al. 2016). Furthermore,
332 pyradoketosite highlights the limits of laboratory experiments trying to synthesize complex sulfides
333 to reproduce ore mineral assemblages. As previously discussed by Keighin and Honea (1969), the
334 slowness of reaction rates below 300°C requires very long-term experiments for achieving
335 equilibrium assemblages, thus representing an important limit to the study of low-*T* ore
336 associations. Consequently, the accurate mineralogical investigation of natural occurrences, where
337 the "synthesis experiments" performed by nature did not suffer from the time constraints typical of
338 human activities, remains a precious and irreplaceable way to discover novel crystal structures and
339 to find complex, unpredictable phases, whose genesis can be related to the wide range of possible
340 *P-T-X* conditions occurring on Earth (e.g., Bindi et al. 2020).

341 Pyradoketosite, the new Ag_3SbS_3 polymorph, is thus a good example of the usefulness of
342 looking for and studying new mineral species.

343 Finally, even if it is undeniably true that to understand and get a first plausible picture of most
344 of the geological phenomena occurring on our planet a dozen minerals might be considered
345 sufficient, we think that rare phases can help to provide a more exhaustive scenario of the Earth

346 dynamics. In other words, with the well-known rock-forming minerals you get an unquestionably
347 correct picture, but still incomplete. Rare phases, and the stories they tell us, can shed light on
348 unusual geological processes and provide the hints to refine and progressively improve the scenario
349 itself.
350

351 ## ACKNOWLEDGMENTS

352 A. Dini is acknowledged for useful discussions. The University Centrum for Applied
353 Geosciences (UCAG) is thanked for the access to the "Eugen F. Stumpfl" electron microprobe
354 laboratory. This research was financially supported by the Ministero dell'Istruzione, Università e
355 Ricerca through the project PRIN 2017 "TEOREM – deciphering geological processes using
356 Terrestrial and Extraterrestrial ORE Minerals", prot. 2017AK8C32.
357 The comments of the Associate Editor Aaron J. Lussier, of Frantisek Laufek, and of two
358 anonymous reviewers were useful for improving the original manuscript.
359

360 ## REFERENCES

361 Adler, D. (1980) Threshold switching in chalcogenide-glass thin films. Journal of Applied Physics
362 51, 3289.

363 Aspiala, M., Tesfaye, F., and Taskinen, P. (2016) Thermodynamic study in the Ag–Sb–S system by
364 the EMF method. Journal of Chemical Thermodynamics, 98, 361-366.

365 Barstad, J. (1959) Phase relations in the system Ag-Sb-S at 400°C. Acta Chemica Scandinavica, 13,
366 1703-1708.

367 Biagioni, C., Bonaccorsi, E., Moëlo, Y., Orlandi, P., Bindi, L., D'Orazio, M., and Vezzoni, S.
368 (2014) Mercury-arsenic sulfosalts from the Apuan Alps (Tuscany, Italy). II. Arsiccioite,
369 $AgHg_2TlAs_2S_6$, a new mineral from the Monte Arsiccio mine: occurrence, crystal structure
370 and crystal chemistry of the routhierite isotypic series. Mineralogical Magazine, 78, 101-117.

371 Biagioni, C., Moëlo, Y., Orlandi, P., and Paar, W.H. (2018) Lead-antimony sulfosalts from Tuscany
372 (Italy). XIII. Andreadiniite, $CuAg_7HgPb_7Sb_{24}S_{48}$, a new oversubstituted (Cu,Hg)-rich member
373 of the andorite homeotypic series from the Monte Arsiccio mine, Apuan Alps. European
374 Journal of Mineralogy, 30, 1021-1035.

375 Biagioni, C., D'Orazio, M., Fulignati, P., George, L.L., Mauro, D., and Zaccarini, F. (2020a)
376 Sulfide melts in ore deposits from low-grade metamorphic settings: Insights from fluid and
377 Tl-rich sulfosalt microinclusions from the Monte Arsiccio mine (Apuan Alps, Tuscany, Italy).
378 Ore Geology Reviews, 123, 103589.

379 Biagioni, C., George, L.L., Cook, N.J., Makovicky, E., Moëlo, Y., Pasero, M., Sejkora, J., Stanley,
380 C.J., Welch, M.D., and Bosi, F. (2020b) The tetrahedrite group: Nomenclature and
381 classification. American Mineralogist, 105, 109–122.

382 Biagioni, C., Zaccarini, F., Roth, P., and Bindi, L. (2020c) Progress in the knowledge of 'ruby
383 silvers': New structural and chemical data of pyrostilpnite, Ag_3SbS_3. Mineralogical Magazine,
384 84, 463-467.

385 Bindi, L., and Biagioni, C. (2018) A crystallographic excursion in the extraordinary world of
386 minerals: the case of Cu- and Ag-rich sulfosalts. Acta Crystallographica, B74, 527-538.
387 Bindi, L., and Evain, M. (2007) Gram-Charlier development of the atomic displacement factors into
388 mineral structures: The case of samsonite, $Ag_4MnSb_2S_6$. American Mineralogist, 92, 886-891.
389 Bindi, L., Evain, M., and Menchetti, S. (2007) Complex twinning, polytypism and disorder
390 phenomena in the crystal structures of antimonpearceite and arsenpolybasite. Canadian
391 Mineralogist, 45, 321-333.
392 Bindi, L., Pratesi, G., and Spry, P.G. (2010) Crystallographic and chemical constraints on the nature
393 of the proustite-pyrargyrite solid-solution series. American Mineralogist, 95, 1725-1729.
394 Bindi, L., Nestola, F., Graeser, S., Tropper, P., and Raber, T. (2015) Eckerite, Ag_2CuAsS_3, a new
395 Cu-bearing sulfosalt from Lengenbach quarry, Binn valley, Switzerland: description and
396 crystal structure. Mineralogical Magazine, 79, 687-694.
397 Bindi, L., Nespolo, M., Krivovichev, S.V., Chapuis, G., and Biagioni, C. (2020) Producing highly
398 complicated materials. Nature does it better. Reports on Progress in Physics, 83, 106501.
399 Brese, N.E., and O'Keeffe, M. (1991) Bond-valence parameters for solids. Acta Crystallographica,
400 B47, 192-197.
401 Bruker AXS Inc. (2016) APEX 3. Bruker Advanced X-ray Solutions, Madison, Wisconsin, USA.
402 Chang, L.L.Y. (1963) Dimorphic relation in Ag_3SbS_3. American Mineralogist, 48, 429–432.
403 Criddle, A.J., and Stanley, C.J., Eds. (1986) The Quantitative Data File for Ore Minerals of the
404 Commission on Ore Microscopy of the International Mineralogical Association (2^{nd} Edition).
405 British Museum (Natural History), 420 p.
406 Effenberger, H., Paar, W.H., Topa, D., Criddle, A.J., and Fleck, M. (2002) The new mineral
407 baumstarkite and a structural reinvestigation of aramayoite and miargyrite. American
408 Mineralogist, 87, 753–764.

Engel, P., and Nowacki, W. (1966) Die Verfeinerung der Kristallstruktur von Proustit, Ag_3AsS_3, und Pyrargyrit, Ag_3SbS_3. Neues Jahrbuch für Mineralogie, Monatshefte, 1966, 181–184.

Goodell, P.C. (1975) Binary and ternary sulphosalt assemblages in the Cu_2S-Ag_2S-PbS-As_2S_3-Sb_2S_3-Bi_2S_3 system. Canadian Mineralogist, 13, 27-42.

Hazen, R.M., and Ausubel, J.H. (2016) On the nature and significance of rarity in mineralogy. American Mineralogist, 101, 1245-1251.

Hoda, S.N., and Chang, L.L.Y. (1975) Phase relations in the system PbS–Ag_2S–Sb_2S_3 and PbS–Ag_2S–Bi_2S_3. American Mineralogist 60, 621-623.

Huber, S., Preitschaft, C., and Pfitzner, A. (2012) Preparation, crystal structure, electronic structure, impedance spectroscopy and Raman spectroscopy of Li_3SbS_3 and Li_3AsS_3. Zeitschrift für anorganische und allgemeine Chemie, 638, 2542-2548.

Johnson, C.K., and Levy, H.A. (1974) International Tables for X-ray Crystallography, edited by J. A. Ibers and W. C. Hamilton, Vol. IV, pp. 311-336. Birmingham: Kynoch Press.

Kanatzidis, M.G., and Chou, J.-H. (1996) Isolation of β-Ag_3AsSe_3, $(Me_3NH)[Ag_3As_2Se_5]$, $K_5Ag_2As_3Se_9$, and $KAg_3As_2S_5$: novel solid state silver thio- and selenoarsenates from solvento-thermal synthesis. Journal of Solid State Chemistry, 127, 186-201.

Keighin, C.W., and Honea, R.M. (1969) The system Ag–Sb–S from 600°C to 200°C. Mineralium Deposita, 4, 153–171.

Kihara, K., and Matsumoto, T. (1986) Refinements of Ag_3AsSe_3 based on high-order thermal-motion tensors. Zeitschrift für Kristallographie 177, 211-217.

Kitakaze, A., Itoh, H., Komatsu, R., and Higuchi, Y. (2006) Baumstarkite from the Koryu mine, Hokkaido, Japan. Canadian Mineralogist, 50, 101–109.

Kocman, V., and Nuffield, E.W. (1973) The crystal structure of wittichenite, Cu_3BiS_3. Acta Crystallographica, B29, 2528-2535.

Kraus, W., and Nolze, G. (1996) PowderCell – a program for the representation and manipulation of crystal structures and calculation of the resulting X-ray powder patterns. Journal of Applied Crystallography, 29, 301-303.

Kutoglu, A. (1968) Die Struktur des Pyrostilpnits (Feuerblende) Ag_3SbS_3. Neues Jahrbuch für Mineralogie, Monatshefte, 1968, 145–160.

Lange, B., Scholz, F., Bautsch, H.-J., Damaschun, F., and Wappler, G. (1993) Thermodynamics of xanthoconite-proustite and pyrostilpnite-pyrargyrite phase transition as determined by abrasive stripping voltammetry. Physics and Chemistry of Minerals 19, 486-491.

Laufek, F., Sejkora, J., and Dušek, M. (2010) The role of silver in the crystal structure of pyrargyrite: single crystal X-ray diffraction study. Journal of Geosciences, 55, 161–167.

Leitl, M., Pfitzner, A., and Bindi, L. (2009) Preferred ion diffusion pathways and activation energies for Ag in the crystal structure of stephanite, Ag_5SbS_4. Mineralogical Magazine, 73, 17–26.

Makovicky, E. (1997) Modular crystal chemistry of sulphosalts and other complex sulfides. EMU Notes in Mineralogy, 1, 237-271.

Makovicky, E., and Balić-Žunić, T. (1995) The crystal structure of skinnerite, $P2_1/c$-Cu_3SbS_3, from powder data. Canadian Mineralogist, 33, 655-663.

Makovicky, E., and Topa, D. (2014) Lillianites and andorites: new life for the oldest homologous series of sulfosalts. Mineralogical Magazine, 78, 387–414.

Makovicky, E., and Topa, D. (2015) Crystal chemical formula for sartorite homologues. Mineralogical Magazine, 79, 25–31.

Matzat, E. (1972) Die Kristallstruktur des Wittichenits, Cu_3BiS_3. Tschermaks Mineralogische und Petrographische Mitteilungen, 18, 312-316.

Moëlo, Y., Makovicky, E., Mozgova, N.N., Jambor, J.L., Cook, N., Pring., A., Paar, W.H., Nickel, E.H., Graeser, S., Karup-Møller, S., Balić-Žunić, T., Mumme, W.G., Vurro, F., Topa, D.,

458 Bindi, L., Bente, K., and Shimizu, M. (2008) Sulfosalt systematics: a review. Report of the
459 sulfosalt sub-committee of the IMA Commission on Ore Mineralogy. European Journal of
460 Mineralogy, 20, 7–46.
461 Orlandi, P., Biagioni, C., Bonaccorsi, E., Moëlo, Y., and Paar, W.H. (2012) Lead-antimony sulfosalts
462 from Tuscany (Italy). XII. Boscardinite, $TlPb_4(Sb_7As_2)_{\Sigma 9}S_{18}$, a new mineral species from the
463 Monte Arsiccio mine: occurrence and crystal structure. The Canadian Mineralogist, 50, 235-251.
464 Orlandi, P., Biagioni, C., Moëlo, Y., Bonaccorsi, E., and Paar, W.H. (2013) Lead-antimony sulfosalts
465 from Tuscany (Italy). XIII. Protochabournéite, $\sim Tl_2Pb(Sb_{9-8}As_{1-2})_{\Sigma 10}S_{17}$, from the Monte Arsiccio
466 mine: occurrence, crystal structure and relationship with chabournéite. The Canadian
467 Mineralogist, 51, 475-494.
468 Petříček, V., Dusek, M., and Palatinus, L. (2006) JANA2006, a crystallographic computing system.
469 Institute of Physics, Academy of Sciences of the Czech Republic, Prague, Czech Republic.
470 Pfitzner, A. (1994) Cu_3SbS_3: Zur Kristallstruktur und Polymorphie. Zeitschrift für anorganische und
471 allgemeine Chemie, 620, 1992-1997.
472 Rosenstingl, J., and Pertlik, F. (1993) Neuberechnung der kristallstruktur von natürlichem und
473 synthetischem monoklinen Ag_3AsS_3 (= xanthokon) nebst einer discussion zur symmetrie.
474 Mitteilungen der Österreichischen Mineralogischen Gesellschaft, 138, 9–15.
475 Schönau, K.A., and Redfern, S.A.T. (2002) High-temperature phase transitions, dielectric
476 relaxation, and ionic mobility of proustite, Ag_3AsS_3, and pyrargyrite, Ag_3SbS_3. Journal of
477 Applied Physics, 92, 7415-7424.
478 Sheldrick, G.M. (2015) Crystal structure refinement with SHELX. Acta Crystallographica, C71,
479 3-8.
480 Smith, J.V., Pluth, J.J., and Han, S.X. (1997) Crystal structure refinement of miargyrite, $AgSbS_2$.
481 Mineralogical Magazine, 61, 671–675.

Trueblood, K.N., Bürgi, H.-B., Burzlaff, H., Dunitz, J.D., Gramaccioli, C.M., Schulz, H., Shmueli, U., and Abrahams, S.C. (1996) Atomic Dispacement Parameter Nomenclature. Report of a Subcommittee on Atomic Displacement Parameter Nomenclature. Acta Crystallographica, A52, 770-781.

Yue, C.Y., Zhang, H.P., Lu, X.X., Bai, Y.Q., Shi, H., and Xu, X. (2012) Solvothermal syntheses and characterization of two new silver selenidoantimonates of Ag_3SbSe_3 and Ag_5SbSe_4. Chinese Journal of Structural Chemistry, 35, 227-236.

Walenta, K. (1998) Cuboargyrit, ein neues Silbermineral aus dem Schwarzwald. Lapis, 23, 21–23.

Weil, R., and Hocart, R. (1953) Recherches expérimentales sur la formation des minéraux d'argent. Comptes Rendus du Congrès des Sociétés Savantes de Paris et des Départments, Toulouse, Section des Sciences, 183-188.

Wilson, A.J.C. (1992) International Tables for Crystallography Volume C. Kluwer, Dordrecht.

Zucker, U.H., and Schulz, H.H. (1982) Statistical approaches for the treatment of anharmonic motion in crystals. II. Anharmonic thermal vibrations and effective atomic potentials in the fast ionic conductor lithium nitride (Li_3N). Acta Crystallographica, A38, 568-576.

This is the peer-reviewed, final accepted version for American Mineralogist, published by the Mineralogical Society of America.
The published version is subject to change. Cite as Authors (Year) Title. American Mineralogist, in press.
DOI: https://doi.org/10.2138/am-2022-8136. http://www.minsocam.org/

TABLE CAPTIONS

Table 1 – Reflectance data (%) for pyradoketosite in air.

Table 2 – Electron-microprobe data (mean of 5 spot analyses, in wt%) of pyradoketosite and atoms per formula unit (apfu) on the basis of 4 (Ag+Sb) apfu.

Table 3 – Observed and calculated X-ray powder diffraction data for pyradoketosite. Intensity and d_{hkl} were calculated using the software *PowderCell*2.3 (Kraus and Nolze 1996) on the basis of the refined structural model. Only reflections with $I_{calc} > 10$ are listed, if not observed. The five strongest calculated reflections are given in bold. Observed intensities were visually estimated (s = strong; mw = medium-weak; w = weak).

Table 4 – Crystal data and summary of parameters describing data collection and refinement for pyradoketosite.

Table 5 – Selected bond distances (in Å) for pyradoketosite.

Table 6 – Bond valence sums (in valence units, v.u.) for pyradoketosite.

Table 7 – Natural and synthetic compounds chemically related to pyradoketosite.

Table 8 – Comparison of unit-cell parameters of members of the wittichenite-skinnerite group with parameters of the supercell of pyradoketosite (see dotted lines in Figure 5).

FIGURE CAPTIONS

Fig. 1 – Pyradoketosite, striated acicular crystals, orange in color (a). Scanning electron microscope image shows the association with equant pyrargyrite and probable tabular pyrostilpnite (b). Sant'Olga tunnel, Monte Arsiccio mine, Apuan Alps, Tuscany, Italy. Holotype material.

Fig. 2 – Reflectance spectrum of pyradoketosite (square), compared with those of pyrargyrite (triangles) and pyrostilpnite (circles). R_1 and R_2 are shown as dotted and dashed lines, respectively. Data for pyrargyrite and pyrostilpnite are after Criddle and Stanley (1986).

Fig. 3 – Crystal structure of pyradoketosite projected down **b**. The organization of SbS_3 groups in two {101} layers having different polarity is shown (arrows indicate the orientation of SbS_3 pyramids). Numbers indicate the Ag (violet) and Sb (green) sites. Dashed red lines indicate the unit cell, whereas blue dashed lines highlight {-102} layers.

Fig. 4 – Organization of {-102} layers [without marginal Ag(5) and Ag(8) atoms].

Fig. 5 – The {101} layered organization of pyradoketosite as seen down **b**. Grey dotted lines show two unit cells, whereas dotted red lines represent the supercell discussed in the text. Numbers "2"

529 and "3" indicate the Ag_2S_2 and Ag_3S_2 groups. Double black arrows show the Ag(3) pairing across
530 the A layers.
531 **Fig. 6** – Crystal structures of wittichenite (a), skinnerite (b), and Li_3SbS_3 (c) as seen down **b**.
532

533 **Table 1** – Reflectance data (%) for pyradoketosite in air.

λ/nm	R_1	R_2	λ/nm	R_1	R_2
400	36.0	36.9	560	29.8	30.3
420	35.0	35.6	580	29.2	29.8
440	34.0	34.3	**589**	**29.0**	**29.6**
460	33.0	33.3	600	28.7	29.3
470	**32.8**	**32.9**	620	28.3	29.0
480	32.2	32.4	640	27.7	28.6
500	30.9	31.9	**650**	**27.5**	**28.4**
520	30.9	31.3	660	27.2	28.2
540	30.4	30.8	680	26.9	28.0
546	**30.2**	**30.7**	700	26.7	27.9

534 Note: data for the four COM wavelengths are given in bold.

535
536

537 **Table 2** – Electron-microprobe data (mean of 5 spot analyses, in wt%) of pyradoketosite and atoms
538 per formula unit (apfu) on the basis of 4 (Ag+Sb) apfu.

Element	wt%	Range	e.s.d.
Ag	59.81	58.90 – 60.21	0.47
Sb	22.63	22.41 – 22.87	0.19
S	17.78	17.55 – 17.92	0.14
Total	100.21	99.31 – 100.66	0.50
	apfu (ΣMe = 4)	Range	e.s.d.
Ag	2.996	2.976 – 3.007	0.011
Sb	1.004	0.993 – 1.024	0.011
S	2.996	2.983 – 3.015	0.015
Ev (%)	0.3	-0.7 – 1.4	0.7

539 Note: $Ev(\%) = [\Sigma(\text{val}+) - \Sigma(\text{val}-)] \times 100 / \Sigma(\text{val}-)$.

540

This is the peer-reviewed, final accepted version for American Mineralogist, published by the Mineralogical Society of America.
The published version is subject to change. Cite as Authors (Year) Title. American Mineralogist, in press.
DOI: https://doi.org/10.2138/am-2022-8136. http://www.minsocam.org/

Table 3 – Observed and calculated X-ray powder diffraction data for pyradoketosite. Intensity and d_{hkl} were calculated using the software *PowderCell*2.3 (Kraus and Nolze 1996) on the basis of the refined structural model. Only reflections with I_{calc} > 10 are listed, if not observed. The five strongest calculated reflections are given in bold. Observed intensities were visually estimated (s = strong; mw = medium-weak; w = weak).

I_{obs}	d_{obs}	I_{calc}	d_{calc}	*h k l*	I_{obs}	d_{obs}	I_{calc}	d_{calc}	*h k l*
w	6.4	10	6.533	0 1 1	w	2.750	18	2.741	1 2 4
w	4.14	32	4.137	-2 0 4	-	-	13	2.715	3 2 1
-	-	10	4.015	-2 1 3	w	2.654	13	2.683	5 0 1
-	-	10	3.900	-1 1 4			23	2.635	3 1 5
-	-	10	3.893	-3 0 3	-	-	14	2.591	0 2 5
w	3.833	20	3.834	-1 0 5	-	-	27	2.553	-5 1 1
-	-	18	3.553	-2 1 4	-	-	19	2.549	5 1 0
mw	3.381	16	3.395	-3 1 3	mw	2.505	13	2.520	1 2 5
		35	3.355	-1 1 5			18	2.506	-4 1 5
-	-	18	3.267	0 2 2			14	2.503	1 1 7
w	3.198	**81**	**3.198**	**-1 2 2**			15	2.482	-2 1 7
		61	**3.193**	**3 1 3**	mw	2.441	17	2.438	-5 1 3
s	3.035	24	3.096	-3 0 5			19	2.436	-4 2 1
		18	3.094	2 2 0	w	2.295	11	2.296	0 3 1
		100	**2.999**	**4 1 1**	mw	2.160	20	2.159	-3 2 6
		57	**2.959**	**2 1 5**			22	2.153	-5 2 1
-	-	23	2.917	2 2 2	-	-	21	2.123	1 2 7
w	2.841	11	2.861	-4 1 3	mw	1.912	15	1.946	-6 0 6
		28	2.835	-2 2 3			11	1.917	-2 0 10
		59	**2.832**	**1 1 6**	mw	1.878	15	1.898	4 3 1
		20	2.827	-3 1 5			15	1.888	2 3 5
-	-	20	2.762	3 2 0	-	-	25	1.799	6 0 6

This is the peer-reviewed, final accepted version for American Mineralogist, published by the Mineralogical Society of America.
The published version is subject to change. Cite as Authors (Year) Title. American Mineralogist, in press.
DOI: https://doi.org/10.2138/am-2022-8136. http://www.minsocam.org/

548 **Table 4** – Crystal data and summary of parameters describing data collection and refinement for
549 pyradoketosite.

550
551
552

Crystal data	
Crystal size (mm)	0.075 × 0.015 × 0.010
Cell setting, space group	Monoclinic, $P2_1/n$
a (Å)	13.7510(15)
b (Å)	6.9350(6)
c (Å)	19.555(2)
β (°)	94.807(4)
V (Å^3)	1858.3(3)
Z	12
Data collection and refinement	
Radiation, wavelength (Å)	Mo $K\alpha$, λ = 0.71073
Temperature (K)	293
$2\theta_{max}$ (°)	52.98
Measured reflections	29750
Unique reflections	3854
Reflections with $F_o > 4\sigma(F_o)$	2682
R_{int}	0.1030
$R\sigma$	0.0628
Range of h, k, l	$-17 \le h \le 17$, $-8 \le k \le 8$, $-24 \le l \le 24$
R [$F_o > 4\sigma(F_o)$]	0.0626
R (all data)	0.1005
wR (on F_o^2)	0.1341
Goof	1.082
Number of least-squares parameters	191
Maximum and minimum residual peak (e Å^{-3})	3.09 [at 1.00 Å from Ag(8)] -2.93 [at 0.86 Å from Ag(8)]

This is the peer-reviewed, final accepted version for American Mineralogist, published by the Mineralogical Society of America.
The published version is subject to change. Cite as Authors (Year) Title. American Mineralogist, in press.
DOI: https://doi.org/10.2138/am-2022-8136. http://www.minsocam.org/

553 **Table 5** – Selected bond distances (in Å) for pyradoketosite.

Ag(1)	– S(7)	2.507(5)	Ag(2)	– S(4)	2.464(5)	Ag(3)	– S(9)	2.468(4)
	– S(1)	2.513(4)		– S(4)	2.471(5)		– S(6)	2.650(5)
	– S(5)	2.530(4)		– S(7)	2.715(5)		– S(5)	2.651(4)
	– S(8)	2.963(5)		– S(8)	2.865(5)		average	2.590
	average	2.628		average	2.629			
Ag(4)	– S(8)	2.466(5)	Ag(5)	– S(5)	2.475(5)	Ag(6)	– S(2)	2.512(4)
	– S(3)	2.511(4)		– S(7)	2.512(5		– S(1)	2.547(5)
	– S(6)	2.648(5)		– S(1)	2.575(4)		– S(9)	2.622(4)
	average	2.541		average	2.521		average	2.560
Ag(7)	– S(3)	2.477(5)	Ag(8)	– S(3)	2.508(4)	Ag(9)	– S(8)	2.483(5)
	– S(6)	2.532(5)		– S(7)	2.516(5)		– S(2)	2.533(5)
	– S(9)	2.594(4)		– S(6)	2.572(5)		– S(2)	2.559(5)
	average	2.534		average	2.532		average	2.525
Sb(1)	– S(2)	2.407(4)	Sb(2)	– S(4)	2.425(4)	Sb(3)	– S(5)	2.453(4)
	– S(8)	2.434(4)		– S(7)	2.460(4)		– S(9)	2.468(4)
	– S(3)	2.445(4)		– S(1)	2.463(4)		– S(6)	2.474(4)
	average	2.429		average	2.449		average	2.465

554

555

556 **Table 6** – Bond valence sums (in valence units, v.u.) for pyradoketosite.

Site	S(1)	S(2)	S(3)	S(4)	S(5)	S(6)	S(7)	S(8)	S(9)	Σcations
Ag(1)	0.37				0.36		0.38	0.11		1.22
Ag(2)				0.43 0.42			0.22	0.14		1.21
Ag(3)					0.26	0.26			0.42	0.94
Ag(4)			0.38			0.26		0.43		1.07
Ag(5)	0.32				0.42		0.38			1.12
Ag(6)	0.34	0.38							0.29	1.01
Ag(7)			0.41			0.36			0.30	1.07
Ag(8)			0.38			0.32	0.37			1.07
Ag(9)		0.36 0.33						0.41		1.10
Sb(1)		1.12	1.03					1.04		3.19
Sb(2)	0.97			1.07			0.97			3.01
Sb(3)					0.99	0.94			0.95	2.88
Σanions	2.00	2.19	2.20	1.92	2.03	2.14	2.32	2.13	1.96	

557

558

This is the peer-reviewed, final accepted version for American Mineralogist, published by the Mineralogical Society of America.
The published version is subject to change. Cite as Authors (Year) Title. American Mineralogist, in press.
DOI: https://doi.org/10.2138/am-2022-8136. http://www.minsocam.org/

559 **Table 7** – Natural and synthetic compounds chemically related to pyradoketosite.

Name	Chemical formula	*a* (Å)	*b* (Å)	*c* (Å)	α (°)	β (°)	γ (°)	*V* (Å^3)	S.g.	*Z*	Ref.
Eckerite	$CuAg_2AsS_3$	11.86	6.23	16.68	90	110.8	90	1152.8	*C*2/*c*	8	[1]
Proustite	Ag_3AsS_3	10.84	10.84	8.72	90	90	120	887.8	*R*3*c*	6	[2]
Pyradoketosite	Ag_3SbS_3	13.75	6.94	19.56	90	94.81	90	1858.3	$P2_1/n$	12	[3]
Pyrargyrite	Ag_3SbS_3	11.05	11.05	8.72	90	90	120	921.6	*R*3*c*	6	[4]
Pyrostilpnite	Ag_3SbS_3	6.86	15.88	6.27	90	117.1	90	608.5	$P2_1/c$	4	[5]
Synthetic	Ag_3AsSe_3	11.30	11.30	8.76	90	90	120	968.4	*R*3*c*	6	[6]
Synthetic	Ag_3AsSe_3	8.11	11.34	20.73	90	90	90	1907	*Pnma*	12	[7]
Synthetic	Ag_3SbSe_3	8.24	11.49	21.22	90	90	90	2009.8	*Pnma*	12	[8]
Xanthoconite	Ag_3AsS_3	12.02	6.26	17.08	90	110.9	90	1200.6	*C*2/*c*	8	[9]

560 S.g. = space group. [1] Bindi *et al*. (2015); [2] Bindi *et al*. (2010); [3] this work; [4] Laufek *et al*. (2010); [5] Biagioni *et*
561 *al*. (2020b); [6] Kihara and Matsumoto (1986); [7] Kanatzidis and Chou (1996); [8] Yue *et al*. (2012); [9] Rosenstingl
562 and Pertlik (1993).

563

This is the peer-reviewed, final accepted version for American Mineralogist, published by the Mineralogical Society of America.
The published version is subject to change. Cite as Authors (Year) Title. American Mineralogist, in press.
DOI: https://doi.org/10.2138/am-2022-8136. http://www.minsocam.org/

564 **Table 8** – Comparison of unit-cell parameters of members of the wittichenite-skinnerite group with
565 parameters of the supercell of pyradoketosite represented in Figure 5.

Name	Chemical formula	S.g.	*Z*	*A'* (Å)	*A''* (Å)	*S* (Å)	Oblique angle (°)	*V* (Å^3)	Ref.
Wittichenite	Cu_3BiS_3	$P2_12_12_1$	4	7.726	6.716	10.935	-	539.16	[1]
Skinnerite	Cu_3SbS_3	$P2_1/c$	8	7.814	13.273	10.242	90.29	1062.27	[2]
Skinnerite	Cu_3SbS_3	$P2_1/c$	8	7.808	13.268	10.233	90.31	1060.09	[3]
Synthetic	Li_3SbS_3	$Pna2_1$	4	7.9671	6.788	10.091	-	545.76	[4]
Synthetic	Li_3AsS_3	$Pna2_1$	4	8.090	6.658	9.868	-	531.52	[4]
Pyradoketosite supercell	Ag_3SbS_3		24	24.831	6.935	22.944	109.84	3716.51	[5]
"average pyradoketosite"	Ag_3SbS_3		4	8.277	6.935	11.472	109.84	619.42	[5]

566 *A*' and *A*'' = in-plane unit-cell parameters; *S* = unit-cell parameter along the stacking direction. The oblique angle is
567 between *A*' and *A''* parameters in skinnerite and between *A*' and *S* in pyradoketosite. S.g. = space group. [1] Kocman
568 and Nuffield (1973); [2] Makovicky and Balić-Žunić (1995); [3] Pfitzner (1994); [4] Huber et al. (2012); [5] this work.

This is the peer-reviewed, final accepted version for American Mineralogist, published by the Mineralogical Society of America.
The published version is subject to change. Cite as Authors (Year) Title. American Mineralogist, in press.
DOI: https://doi.org/10.2138/am-2022-8136. http://www.minsocam.org/

Fig. 1

This is the peer-reviewed, final accepted version for American Mineralogist, published by the Mineralogical Society of America.
The published version is subject to change. Cite as Authors (Year) Title. American Mineralogist, in press.
DOI: https://doi.org/10.2138/am-2022-8136. http://www.minsocam.org/

Fig. 2

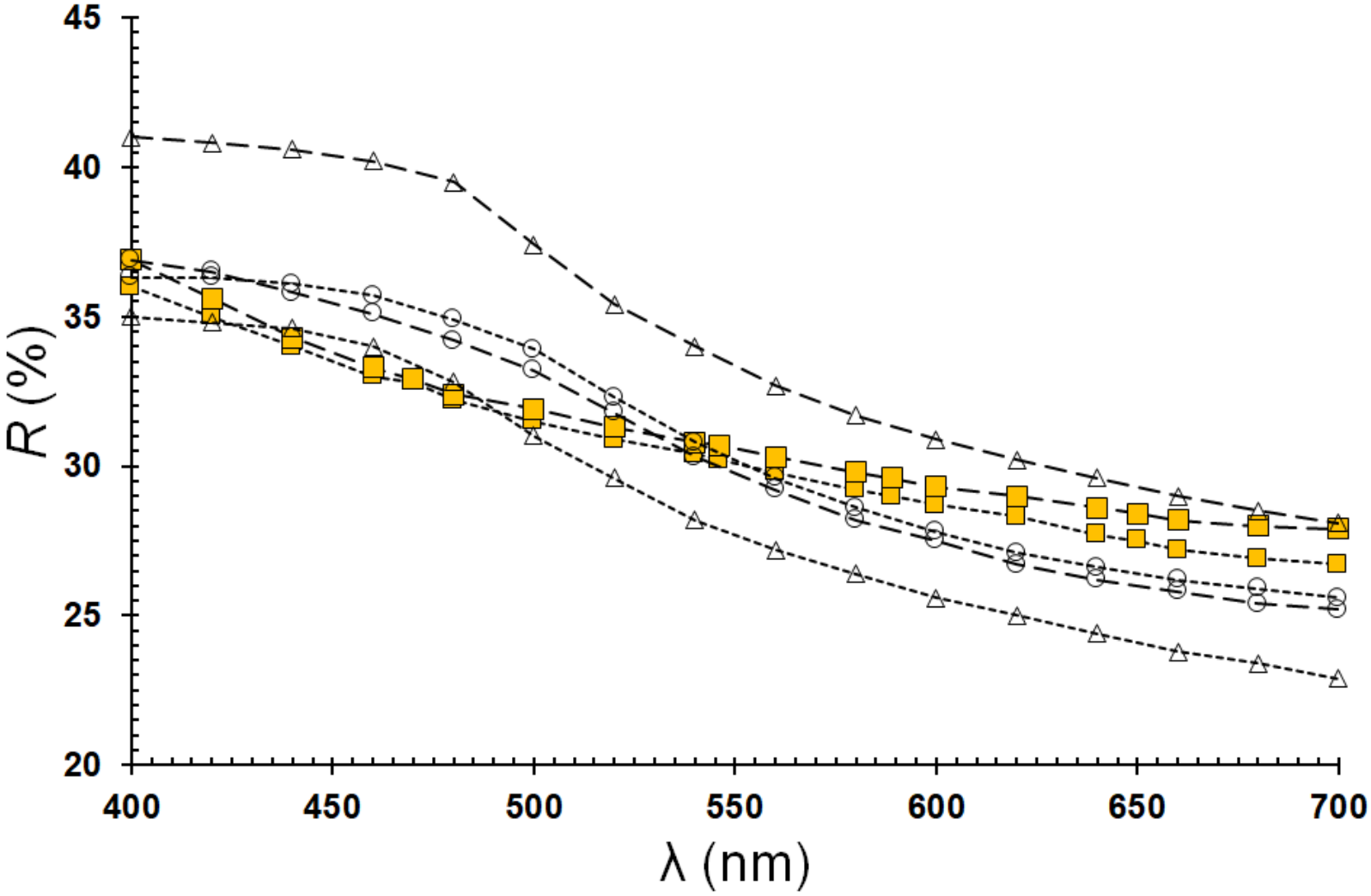

This is the peer-reviewed, final accepted version for American Mineralogist, published by the Mineralogical Society of America.
The published version is subject to change. Cite as Authors (Year) Title. American Mineralogist, in press.
DOI: https://doi.org/10.2138/am-2022-8136. http://www.minsocam.org/

Fig. 3

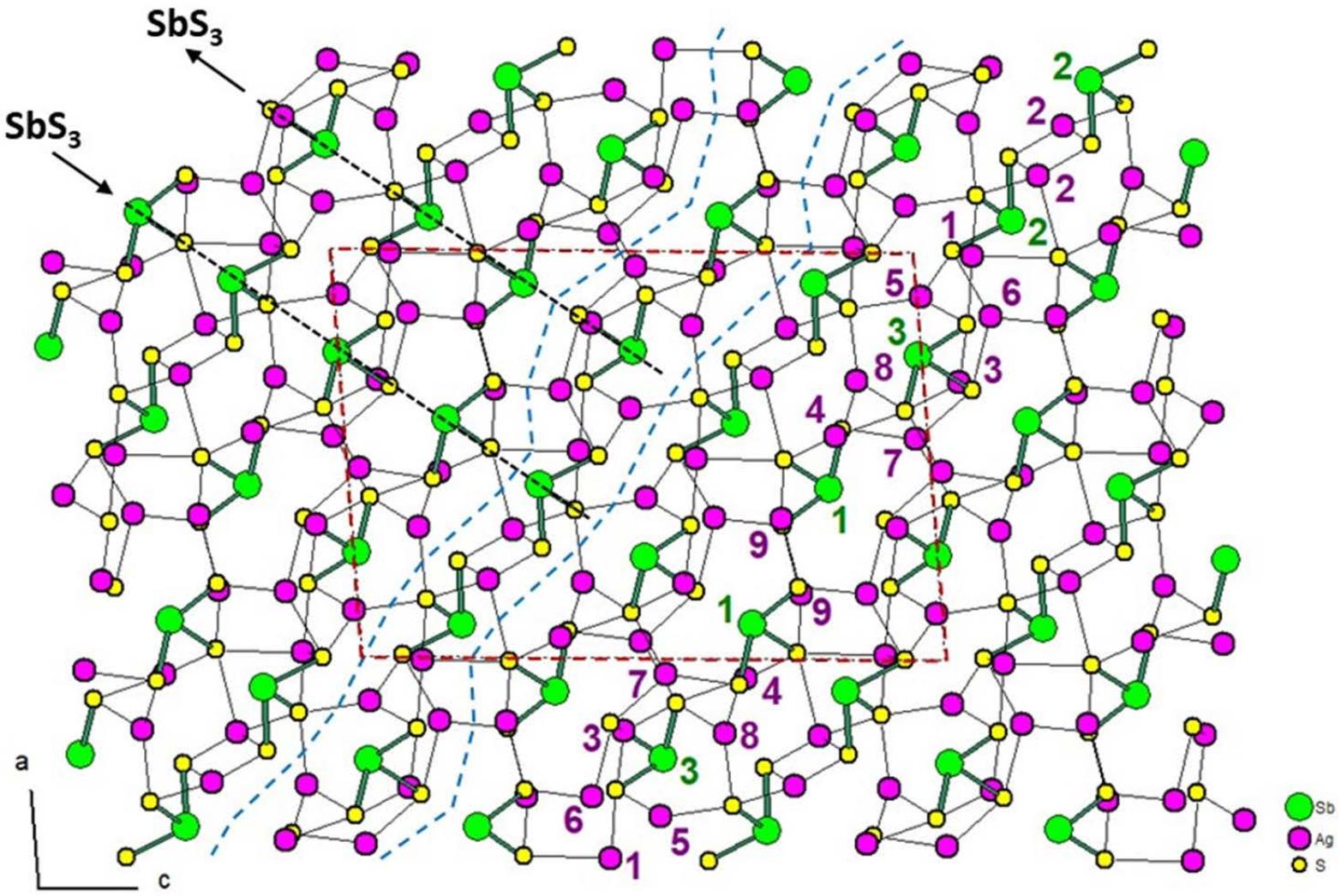

This is the peer-reviewed, final accepted version for American Mineralogist, published by the Mineralogical Society of America.
The published version is subject to change. Cite as Authors (Year) Title. American Mineralogist, in press.
DOI: https://doi.org/10.2138/am-2022-8136. http://www.minsocam.org/

Fig. 4

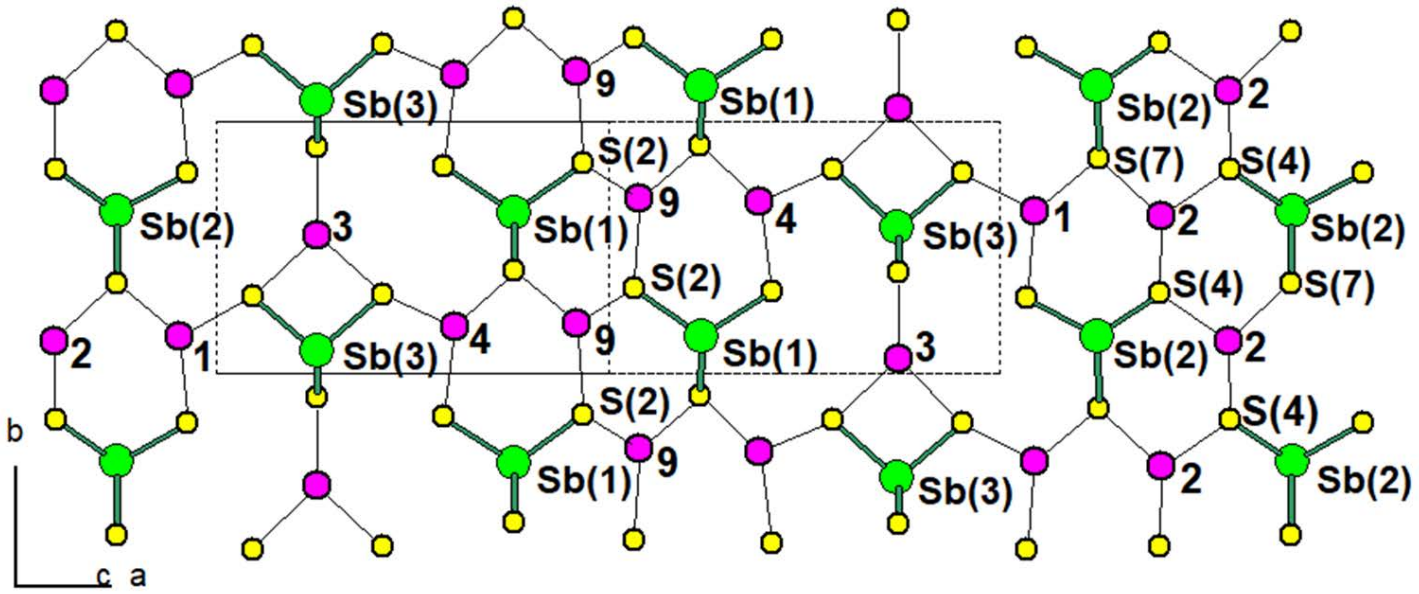

This is the peer-reviewed, final accepted version for American Mineralogist, published by the Mineralogical Society of America.
The published version is subject to change. Cite as Authors (Year) Title. American Mineralogist, in press.
DOI: https://doi.org/10.2138/am-2022-8136. http://www.minsocam.org/

Fig. 5

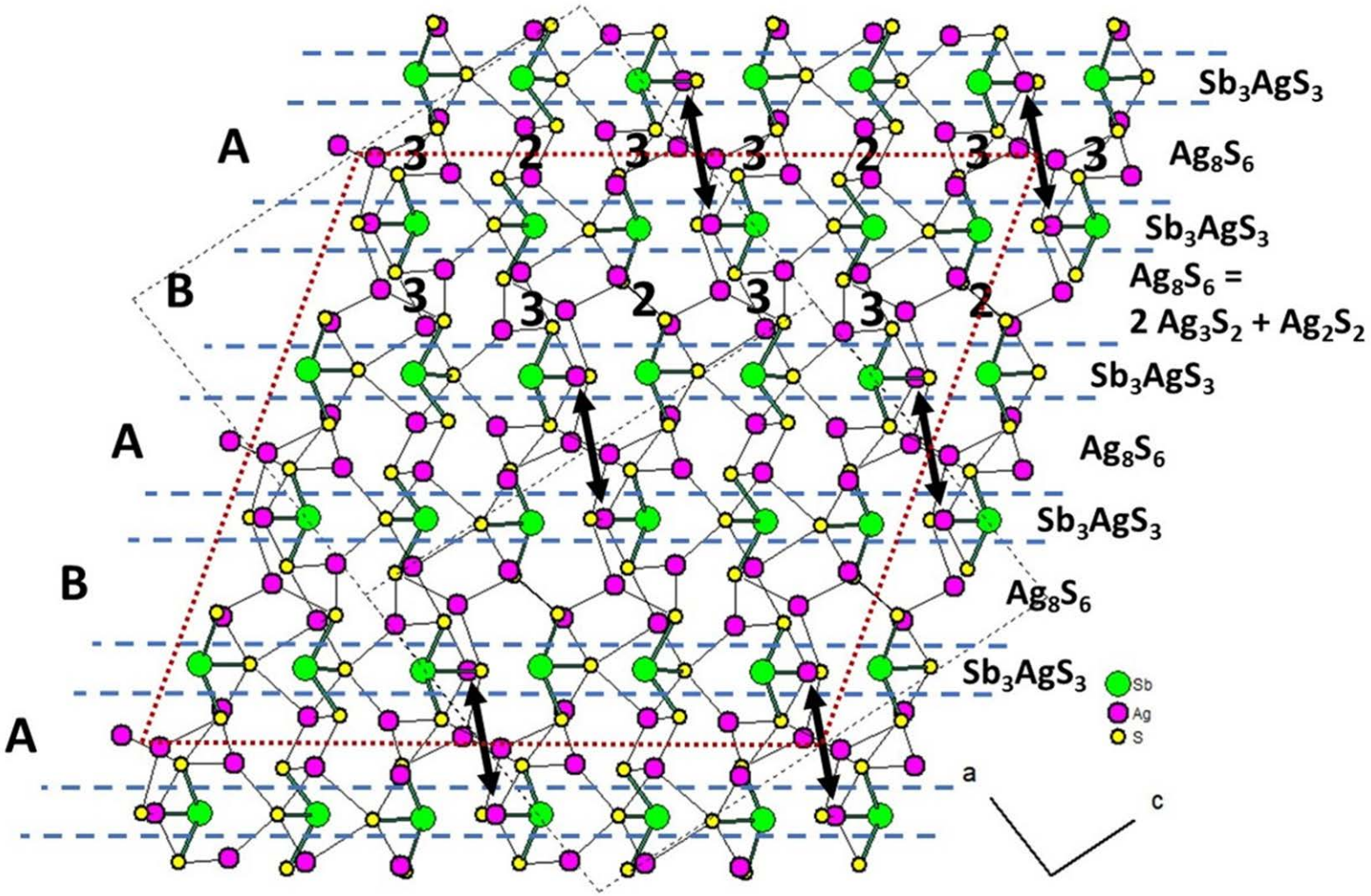

Fig. 6

(a)

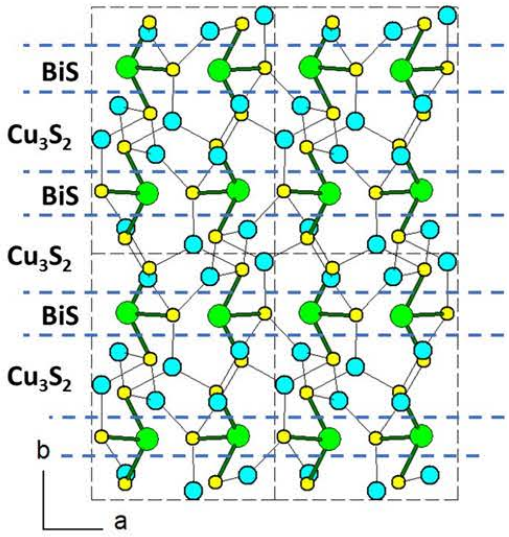

(b)

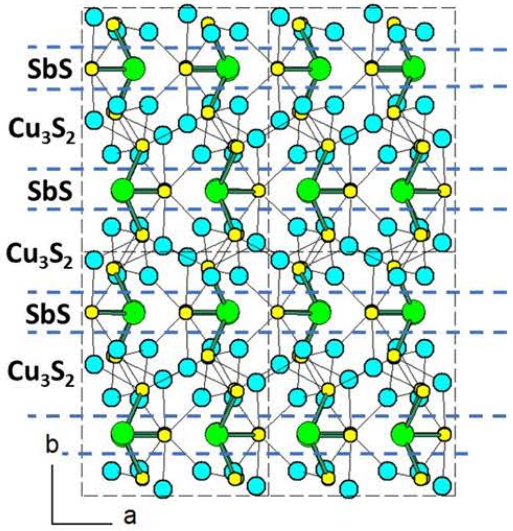

(c)